IOP Publishing Measurement Science and Technology
Meas. Sci. Technol. 31 (2020) 015901 (9pp) https://doi.org/10.1088/1361-6501/ab3b2d

Ultra-fast measurement circuit for transient space charge limited current in organic semiconductor thin films

Karsten Rojek, Roland Schmechel and Niels Benson

Institute of Technology for Nanostructures and CENIDE, University Duisburg-Essen, Bismarckstrasse 81, 47057, Duisburg, Germany

E-mail: karsten.rojek@uni-due.de, roland.schmechel@uni-due.de and niels.benson@uni-due.de

Received 18 April 2019, revised 9 August 2019
Accepted for publication 14 August 2019
Published 22 October 2019

Abstract

The charge carrier mobility is a crucial parameter determining the device performance for numerous different semiconductor applications. Consequently, an accurate measurement of this quantity is crucial. For this purpose, the transient space charge limited current (SCLC) method is commonly applied and is preferable over, for example, Hall or field effect measurements, as the analyzed current direction is in line with typical device architectures. For the transient SCLC method, a voltage step is applied and the transit time of injected charge carriers is determined using displacement currents. Consequently, the difficulty of this method is the use of an adequate RC time constant for the sample charging, as it needs to be much shorter than the transit time. This parameter generally limits the application of transient SCLC strongly, in terms of obtainable charge carrier mobility or minimum required film thickness. Here, we demonstrate a measurement circuit with a low RC time constant, which works in a wide current range (1 μA–0.5 A) and thus allows for significant flexibility in terms of minimum film thickness or detectable charge carrier mobility. The circuit is fast enough to measure, for example, charge carrier mobilities of up to 10^{-4} cm^2 Vs^{-1} for a 76 nm thick 4,4',4''-Tris[phenyl(m-tolyl)amino]triphenylamine (MTDATA) layer, without using limited bridge circuitry. For this purpose, a capacitor coupled fast transistor switch generates a voltage step to avoid voltage oscillations and a fast operational amplifier is used for amplification of the voltage over a variable measurement resistor. We demonstrate the circuit working principle by measuring benchmarked MTDATA diodes and discuss its range of application.

Keywords: mobility, space charge limited current, organic semiconductor, transient space charge limited current, dark injection space charge limited current, measurement circuit, MTDATA

Supplementary material for this article is available online

(Some figures may appear in colour only in the online journal)

1. Introduction

The charge carrier mobility is a crucial parameter to evaluate the device performance for numerous different semiconductor applications [1, 2]. For the determination of the mobility, measuring the steady state or transient space charge limited current (SCLC) is a widely used technique [1, 3]. For example, light emitting or photovoltaic applications, measuring the SCLC in either way, is preferable over other methods such as field- or Hall-effect measurements, as the charge carrier mobility is determined in line with the current transport direction of typical device architectures [1, 3–5]. This is also true for time of flight (ToF) measurements [3]. However, the ToF method has higher requirements for the sample structure to

ensure efficient light incorporation. Additionally, ToF measures small currents compared to the SCLC methods and are typically smaller then the currents used in typical devices.

Although the steady state or transient SCLC method is the appropriate choice for determining the mobility for the mentioned applications, both methods implicate challenges. Non-ideal devices make the determination and reproducibility of the mobility from a single current-voltage measurement of steady state SCLC measurements difficult [1]. For confirmation of determined mobility values, the comparison to transient SCLC measurements at the same sample is reasonable and results in a self-consistent measurement method. This allows for a more accurate evaluation of the mobility and at the same time gives information about the occurring non-idealities like trap occurrence, injection barriers and amount of minority charge carriers [6–9]. Hereby, the transient SCLC method is more precise concerning the determination of the mobility from a pronounced current peak. However, a major drawback is the need for a very low RC time constant for charging the device fast, which is explained in the following.

For the purpose of transient SCLC, a voltage step is applied to a unipolar device and the time dependent current is measured. Ideally, a current peak occurs, when the first injected charge carriers have traveled through the sample, which can be directly correlated with the mobility. This technique was widely used for thick layers or low mobilities resulting in large transit times [3, 4, 7, 8, 10]. However, semiconductors are often deposited in thin layers for thin film device applications. One example are organic semiconductors processed from solution. Such thin films typically have high sample capacitances, which consequently increase the RC time constants for the sample charging. This results in a superposition of charging currents with the relatively fast transient signal, falsifying the measurement or even making it impossible [11]. The sample capacitance can only be reduced by changing the sample area. However, this is limited by an increase in sample resistance and a consequent current signal reduction, causing the measurement to be more challenging in respect to the noise level.

Thus, minimizing the serial resistance is crucial for improving the minimum measureable transit time. Additionally, parasitic capacitances in parallel to the device under test, e.g. the capacitance of wires between sample and voltage step generation, have to be reduced. Consequently, the length of wires has to be as short as possible and the use of coaxial cables with a high capacitance has to be avoided. This makes the use of a standard pulse generator with a typical 50 Ω output resistance difficult. Furthermore, the input capacitance and resistance of current measurement devices has to be considered, as well as the resistance of the device under test contact metalization of the device under test. There are approaches for solving this challenge, such as using bridge circuits [3, 12, 13] or an operational amplifier used as a trans-impedance amplifier [13]. However, bridge circuits require a calibration for every new sample and trans-impedance amplifiers directly influence the measurement signal, limiting the usefulness of the measurement [12, 13].

Here, we demonstrate a transient SCLC circuit, which allows low RC time constants even for thin semiconductor layers, and therefore avoids the addressed issues.

2. Theory

In this contribution, the mobility values determined using steady state SCLC are used as a benchmark for the results determined with the developed transient SCLC circuit. Therefore, in the following, the theory behind both techniques is discussed. The general sample structure for measuring SCLC is a semiconductor or isolator layer between two electrodes. One electrode must be injecting majority charge carriers and the other electrode blocking minority charge carrier injection. For the ideal SCLC case, several assumptions are made [1, 9, 13, 14]: (i) the charge injection is efficient, meaning that the injecting contact has a neglectable injection resistance; (ii) the serial resistance of, for example, contact metalization and cables has to be low in comparison to the sample resistance; (iii) the blocking contact is efficient and thus, the device is assumed to be unipolar; (iv) the difference of the electrode work functions is zero, resulting in no build-in field and in a symmetric device; (v) the trapping of charge carriers, doping and a field dependency of the mobility are neglected.

The current voltage relation for the ideal steady state SCLC is then given by the Mott–Gurney law (equation (1)) [15]:

$$J = \frac{9}{8} \cdot \epsilon \cdot \mu \cdot \frac{V^2}{d^3}. \tag{1}$$

Here, J is the current density within the active layer, $\epsilon = \epsilon_r \cdot \epsilon_0$ is the specific dielectric permittivity (ϵ_r) and dielectric constant (ϵ_0), μ the charge carrier mobility, d the thickness of the active layer and V the applied voltage. By fitting equation (1) to a current density-voltage (JV) curve, the mobility can be determined if the active area, ϵ and d are known.

For ideal transient SCLC measurements, a voltage step V_S is applied at time $t = 0$ to the device and the current measured over t. In principle, the first charge carriers injected by this voltage pulse are moved by an, in average, stronger electrical field through the sample than the charge carriers for the steady state case at $t \to \infty$. This results in a transient current peak when the first injected charge carriers arrive at the non-injecting electrode, which is defined as the transit time t_{trans}. Ideally, the peak current is a factor 1.21 higher than in the steady state [4, 16]. The transit time is directly correlated to μ by equation (2) [4, 16, 17]:

$$\mu = 0.786 \cdot \frac{d^2}{V_S \cdot t_{\text{trans}}}. \tag{2}$$

A major difference between the steady state and transient SCLC techniques is their dependency on the electric field strength. The mobility determined using the steady state measurement is a parameter independent of the electrical field strength, which is primarily useful for the material comparison

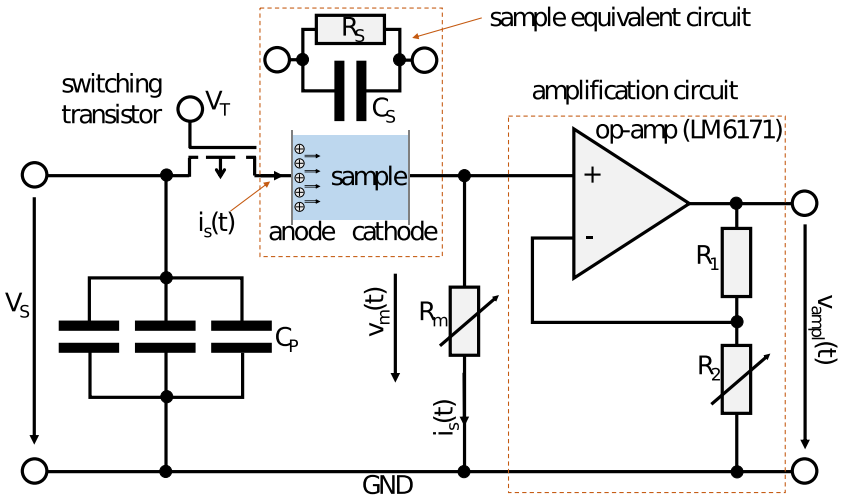

Figure 1. Schematic of the measurement circuit for transient SCLC. The detailed circuit is shown in the supplemental material.

in similar devices [1, 18]. In contrast, the mobility determined by the transient method is correlated to a certain average electrical field strength, making the measurement more precise compared to the steady state method.

However, there are many effects influencing both measurement approaches, which are correlated to non-idealities and which become more dominant for thin layers. These limitations will be discussed in the following, as we demonstrate the measurement limitations of our circuit using semiconductor thin films which show thickness dependent effects. Starting with the steady state SCLC, the relation between current and voltage is ideally $J \propto V^w$, with $w = 2$. For real devices, w is typically larger than 2, mainly due to the influence of trap states [14, 19]. If w is close to 2, a trap state influence on the mobility can be neglected with good approximation [14, 19, 20]. Additionally, w is influenced by several other aspects, which are: the presence of an injection barrier, a field dependence of the mobility, serial resistances, shunt resistances and build-in fields. The effect of these non-idealities varies in dependence on the semiconductor film thickness. An increasing w with thinner layers is attributed to injection limitation [1, 21]. This effect saturates for thick layers, as the contact resistance becomes small when compared to the overall sample resistance. Furthermore, a field dependent mobility, especially for organic semiconductors, can cause higher w, which increases naturally with increasing voltages [11, 21–23]. Therefore, if the charge carrier mobility is determined using equation (1), the mobility is strongly influenced for thinner layers, as injection resistances, serial resistances and build-in field have a higher impact [1, 23]. The discussed effects may cause a strong increase of w up to, for example, 6, where a determination of the mobility with a quadratic fit by equation (1) becomes invalid. However, equation (1) describes the maximum possible current at a given mobility considering non-ideal effects which increase the double logarithmic gradient. Therefore, a fit with equation (1), in a short range of the JV characteristic, can still be considered as a good reference value for the circuit evaluation, as the obtained mobility can be considered as a minimum value.

Moving on to the transient SCLC method, calculating the mobility with the occurring current peak is still possible concerning the discussed non-idealities, although the effects on the calculated mobility are similar. For thin layers, there is still a decrease of the determined mobility by build-in field, injection resistances and serial resistances [11, 17, 24]. Especially, a high serial resistance will cause a high RC time constant resulting in a wide charging current peak. This peak may overlap with the transient peak, falsifying the measurement. However, the field dependence of the mobility is directly visible with transient SCLC, as the mobility is measured for a certain field strength [25]. Furthermore, occurring trap states cause slight shifts of the current peak to higher t_{trans}, giving a parameter for characterization of the influence of trap states [17]. In the case of deep trap states, a slow attenuation of current over much longer time scales than t_{trans} is visible [4, 14, 17].

3. Measurement setup

For the purpose of fast transient SCLC measurements, we have developed the circuit illustrated in figure 1. We use a serial measurement resistance as demonstrated by Staudiegel [26] with an added voltage amplification circuit. The circuit and the sample connectors are implemented on a single printed circuit board (PCB) to reduce cable length and consequently the influence of the measurement environment. The PCB layout is presented in the supplemental material (stacks.iop.org/MST/31/015901/mmedia). The voltage step, which changes the applied voltage on the device under test from 0 V vo V_S, is generated by a fast (maximal 55 ns rise time [27]) switching transistor (IRFR9024NPBF from Infineon Technologies) The gate voltage V_T (in relation to ground potential GND) is equal to V_S prior to the measurement and is set to 0 V at $t = 0$. The details of this switching circuits are shown in the supplementary material. Hereby, V_S is stabilized by a set of capacitors C_P consisting of an electrolyte (100 µF), a foil (0.47 µF) and a ceramic capacitor (0.22 µF). This combination allows for a high total capacitance and simultaneously fast response time

Table 1. The amplification a in dependents of R_m and R_2 and the measurable minimum (i_{min}) and maximum current (i_{max}).

R_m (Ω)	R_2 (Ω)	a (V A^{-1})	i_{min} (mA)	i_{max} (mA)
10	$\rightarrow \infty$	10	1	500
10	174	44.7	1000	330
10	34.8	184	220	81
10	8.06	759	54	20
10	2	3030	3.4	5
300	$\rightarrow \infty$	300	34	50
300	174	1341	7.4	11
300	34.8	5520	1.8	2.7
300	8.06	22 770	0.44	0.66
300	2	90 900	0.11	0.17

preventing oscillations of V_S. The switching transistor is in series with the sample and with the measurement resistance R_m. The voltage drop $v_m(t)$ over this resistance is measured in order to determine the current using Ohm's law (equation (3)):

$$v_m(t) = R_m \cdot i_s(t). \tag{3}$$

As R_m has to be small in order to ensure fast charging times resulting in small $v_m(t)$, an amplification circuit is used with an operational amplifier (LM6171 from Texas Instruments) in combination with the resistances R_1 (600 Ω) and the variable resistance R_2 to define the amplification factor a of the circuit (equation (4)):

$$a = \frac{R_1 + R_2}{R_2} \cdot R_m. \tag{4}$$

This allows us to choose small R_m values down to the order of 10Ω. For the total serial resistance R_{serial} of the sample, including wiring and contact metalization resistances and R_m, this results in a minimal value of 17 Ω. The output voltage of the amplification circuit $v_{ampl}(t)$ is measured by an oscilloscope (UTD2052 from Uni-Trend). The circuit is calibrated by measuring resistances in series with an external ampere meter (Keithley, 4200-SCS), instead of a sample, and correlating the measured current to $v_{ampl}(t)$ using a linear regression fit. Thus, the measured current has a direct correlation with $v_{ampl}(t)$ (equation (5)). The derivation of equations (4) and (5) is given in the supplementary material:

$$v_{ampl}(t) = a \cdot i_s(t). \tag{5}$$

The resistances responsible for signal amplification R_2 and R_m can be adjusted to accommodate a wide current range from 1 µA to 0.5 A (table 1). Additionally, the chosen elements of the circuit limit the current to 0.5 A and VS to 50 V. However, for most amplification factors, the range is limited by the maximum output voltage of the operational amplifier, as well as the noise level of $v_{ampl}(t)$, which is approximately at 10 µ V. The measurement limits of the circuit in dependence of the applied amplification are discussed in the following.

For measuring the transient SCLC using the circuit outlined above, the suitable amplification has to be chosen for every V_S in such way, that the amplified voltage $v_{ampl}(t)$ is in the measurement range. Hereby, the amplification factor influences the bandwidth of the amplification circuit. A high amplification causes a low band width and vice versa. On the one hand, if a high amplification is needed in case of a low current, the low bandwidth can limit the measurement. A slow answer of the amplification circuit to fast current changes such as the charging peak can result in the overlap of charging peak and transient peak. On the other hand, in case of a high bandwidth, operational amplifiers tend to oscillate as a response to fast input voltage changes [27]. To reduce this effect, R_1 is chosen to be as large as possible while a high amplification is still possible by choosing a small R_2 of 2 Ω. For switching between different R_m, optical solid state relays (AQY212EHA, Panasonic) are use because of their very small input capacitance of 0.8 pF. In case of R_2, transistors (NTGD3148NT1G from ON semiconductors) are used as switches. The complete circuit is shown in the supplemental material.

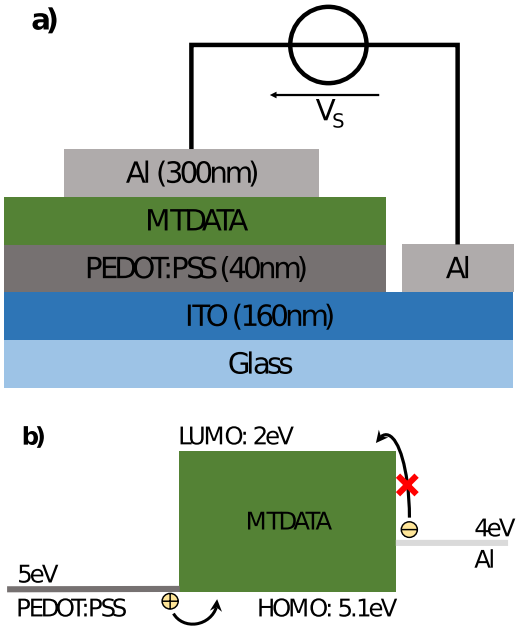

Figure 2. (a) Layer stack of measured devices with varying MTDATA film thicknesses. (b) HOMO and LUMO levels of MTDATA in relation to the work functions of PEDOT:PSS and Al.

4. Samples

The working principle of the developed transient SCLC circuit and its measurement limits is demonstrated using a hole-only organic semiconductor based device, with 4,4',4"-Tris[phenyl(m-tolyl)amino]triphenylamine (MTDATA, from Sigma Aldrich) as the active layer. As MTDATA can be deposited by evaporation, different layer thicknesses are possible with neglectable deviation in the micro structure, making devices with different thicknesses comparable. This is an ideal case to evaluate the working principal of the discussed circuit, as a thin MTDATA layer can demonstrate the minimum transit time t_{trans} measurable by this circuit, while thick layers can be used to proof the correctness of the measurement in comparison to literature data.

Figure 2(a) shows the schematic layer stack of the MTDATA devices. A 40 nm thick layer of

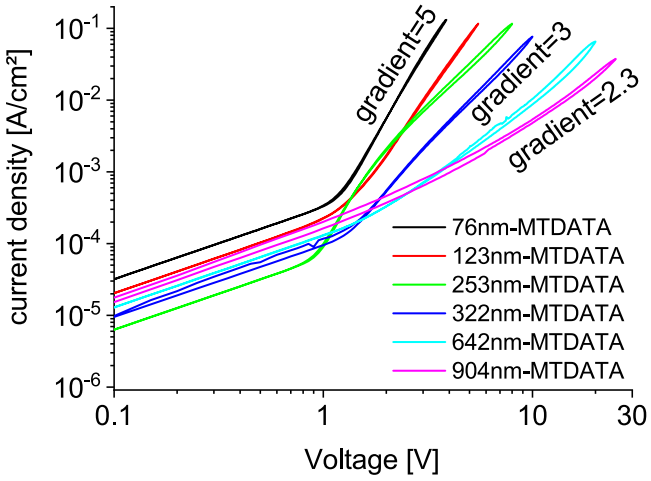

Figure 3. JV characteristics of MTDATA samples with varying semiconductor thin film thicknesses in a double logarithmic plot.

Poly(3,4-ethylenedioxythiophene) polystyrene sulfonate (PEDOT:PSS, HTLsolar Clevios from Haereus) is used for hole injection [3]. PEDOT:PSS has a work function of 5 eV [28], thus there is a good energy alignment to the HOMO (5.1 eV) of the MTDATA [10, 29, 30] (figure 2(b)). For the electron blocking contact, Aluminum (Al) with a work function of 4 eV is used [31, 32]. Considering the LUMO of MTDATA at 2 eV [10, 29, 30], the energy barrier for electron injection is 2 eV. Consequently, this is an effective electron blocking contact [10] resulting in a hole only device.

The measured devices are built as described in the following. The pre-structured indium tin oxide (ITO) glass substrate was commercially available from Naranjo BV, which was pre-treated with UV light and ozone at 110 °C for 15 min prior to the PEDOT:PSS deposition. The solution of PEDOT:PSS was diluted with twice distilled water in the ratio 1:1 and kept in an ultra-sonic bath for 30 min. Right before deposition, the solution was filtered through a 0.45 µm polyvinylidene fluoride (PVDF) filter. The deposition was done by spin coating at 500 rpm for 5 s with subsequent 5000 rpm for 40 s. Afterwards, the samples were tempered at 130 °C for 5 min in ambient atmosphere and another 25 min in nitrogen atmosphere. From this time on, the samples stayed in nitrogen atmosphere at all times. Subsequently, MTDATA was deposited by thermal evaporation with varying thicknesses (76 nm, 123 nm, 253 nm, 322 nm, 642 nm and 904 nm) at a rate between 0.3 and 1.3 Å s^{-1} at a maximum pressure of $1 \cdot 10^{-6}$ mbar. A 300 nm thick Al layer was used as top electrode, which was also thermally evaporated. The deposition of the first 30 nm Al was done with a rate below 1 Å s^{-1} at a maximum pressure of $6 \cdot 10^{-6}$ mbar. The rate was then increased up to 50 Å s^{-1} at $1 \cdot 10^{-5}$ mbar for the remaining 270 nm. The device area of 7.5 mm^2 is defined by the overlap of bottom and top electrodes.

5. Results

The diode (JV) characteristics of the devices under test are illustrated in figure 3 in double logarithmic form. They are only used here, to obtain reference values for the charge carrier mobility determined using the developed transient SCLC circuit. For thick samples (642 nm and 904 nm), the determined gradient of the double logarithmic plots is approximately 2.3, which marginally increases with high voltages. This is the result of the discussed field dependent charge carrier mobility. These samples can be considered almost trap free, as a gradient close to 2 is the result of neglectable trap densities [14, 19, 20]. For thinner layers, the gradient of the JV-characteristic increases up to values of 5. As we do not expect this to be the influence of a change in the semiconductor microstructure, as outlined above, we suggest this to be the influence of an injection limitation with increasing dominance as the semiconductor thickness is reduced. The estimated mobility values using the described steady state approach range from $2.5 \cdot 10^{-5}$ cm^2 Vs^{-1} (for 76 nm) to $1.4 \cdot 10^{-4}$ cm^2 Vs^{-1} (for 904 nm) with an assumed $\epsilon_r = 3$ [1, 19]. This data is used in the following as reference information for the transient SCLC evaluation.

Illustrated in figure 4(a) is an exemplary transient SCLC measurement of the 322 nm thick MTDATA sample for V_S values ranging from 6 V to 14 V, illustrating the challenges associated with the measurement. The vertical dashed lines indicate the positions of t_{trans} for each value of V_S.

For a voltage step with $V_S = 6$ V, there is a smooth peak visible in the transient characteristic, from which the mobility can be calculated using equation (2). The charging peak of this measurement within the first 0.7 µs results in saturation of $v_{\text{ampl}}(t) = 15$ V, which does not influence the actual measurement. The width of this charging peak is the result of the device RC time constant and the bandwidth of the operational amplifier. The RC time constant is estimated by assuming a plate capacitor [33] and the values: $\epsilon_r = 3$ [1, 19], $d = 322$ nm MTDATA, $A = 7.5$ mm^2 as active device area and a serial resistance of 17 Ω. The estimated value is in the order of 11 ns. After approximately 10 times of the RC time constant, thus after 110 ns, the charging peak should have subsided. The apparent broadening of the charging peak, as it has not subsided after 700 ns, results from the low bandwidth and therefore slow response of the amplification circuit. The amplification of 759 A V^{-1} used for $V_S = 6$ V works up to $V_S = 8$ V, as for higher values of V_S, $v_{\text{ampl}}(t)$ is getting close to 15 V and the charging peak starts to overlap the transient peak. Consequently, for $V_S > 8$ V, a lower amplification of 184 A V^{-1} is necessary, which results in a higher bandwidth of the operational amplifier. This, however, results in oscillations, which overlap the actual transient SCLC signal as indicated by the inset of figure 4(a) and as highlighted in figure 4(b) using a reference measurement under open circuit conditions, although the oscillation amplitude is smaller here. This Oscillation originates from the operational amplifier as a consequence of the steep change of $v_m(t)$ during the sample charging. Figure 5 shows the result of an analytical approximation of this charging peak considering only C_s and R_s as shown in the sample equivalent circuit in figure 1. It is obvious, that up to 75 ns the charging current (only C_s) dominates and the sample current (only R_s) can be neglected. The charging current is estimated using the equations (6) (0 to the

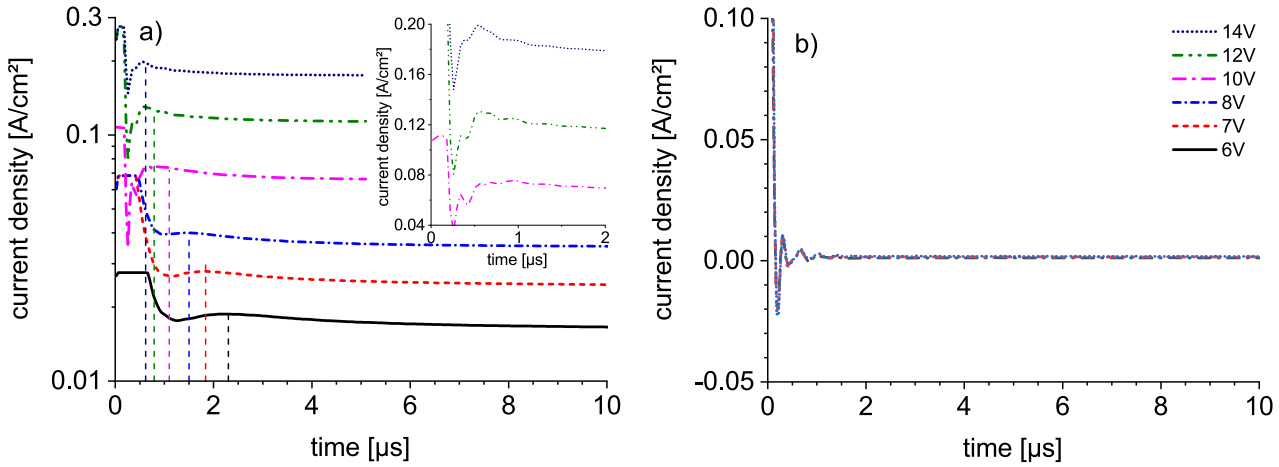

Figure 4. (a) Transient SCLC measurement of a 322 nm thick MTDATA layer with $R_m = 10\ \Omega$. For V_S between 6 V and 8 V, an amplification of 759 A V^{-1} is used and 184 A V^{-1} for $V_S > 8$ V. Low amplification result in oscillation of the operational amplifier, which is shown in the inset. (b) Reference measurement in open circuit condition.

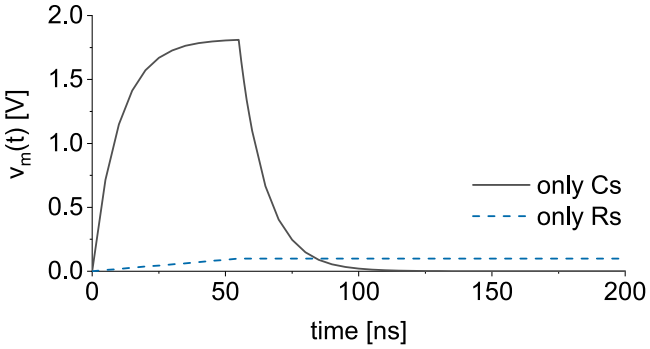

Figure 5. Analytical estimation of the charging peak of the input voltage of the operational amplifier considering either only C_s or R_s of the sample equivalent circuit in figure 1 with: $V_s = 10$ V, $R_s = 1$ kΩ, $C_s = 1$ nF and $R_{\text{serial}} = 10\ \Omega$.

rise time $t_r = 55$ ns) and (7) (above t_r). Hereby, a linear rise of the voltage pulse is assumed, reaching V_s with a gradient of $A = V_s/t_r$. For t_r, the maximum rise time of the switching transistor is considered. The derivation of both equations is shown in the supplementary material and $v_m(t)$ is calculated by $v_m(t) = V_s - v_{C_s,i}(t)$:

$$v_{C_s,1}(t) = A \cdot t - A \cdot R_{\text{serial}} C_s \left(1 - \mathrm{e}^{-\frac{t}{R_{\text{serial}} C_s}}\right) \tag{6}$$

$$v_{C_s,2}(t) = \left(v_{s,1}(t_r) - V_s\right) \cdot \mathrm{e}^{-\frac{t-t_r}{R_{\text{serial}} C_s}} + V_s. \tag{7}$$

The result in figure 4(b) demonstrates a voltage independence of the oscillation, which is most likely caused by the charging of parasitic capacitances of the used elements within the circuit. By subtracting the open circuit measurement from the actual transient measurements, the influence of the oscillation can be reduced, however, not completely avoided. In order to further improve the oscillation suppression, the signals from figure 4(a) are analyzed after open circuit correction in the frequency domain obtained by fast Fourier transformation (FFT) [34] (figure 6(a)).

For low V_S up to 8 V, the amplitude has a smooth, almost linear characteristic. However, for higher voltages several peaks occur which can be ascribed to the discussed oscillations in the time domain. These peaks can be filtered with a low-pass filter using a cut-off frequency f_{cut} just below those peaks, which are indicated by the dots in figure 6(a).

For this, we use the FFT-filter for smoothing curves provided by OriginPro 2018b (OriginLab Corporation). This filter essentially does a linear fit between the start and the end of a user defined range Δt in the time domain. The software subtracts this linear fit from the original data and performs a FFT on the result. The data in the frequency domain is filtered by a parabolic low-pass filter with f_{cut} defined by equation (8). The parabolic form of the low-pass filter is defined by 1 at 0 Hz (no deletion of frequency data) and 0 at f_{cut} (complete deletion of frequency data). Afterwards, the signal is transformed back into time space by reverse FFT and the linear fit is added:

$$\Delta t = \frac{1}{2 f_{\text{cut}}}. \tag{8}$$

The influence of these filters in the time domain is illustrated in figure 6(b). The signal is no longer influenced by parasitic oscillations and the signal analysis can now be conducted without any issues. The challenge of the frequency domain signal correction approach is choosing the correct cut off frequency, as the transient peak maximum required for the charge carrier mobility extraction is slightly influenced in the time domain by this step. To address this issue, the magnitude of this influence was evaluated by changing the cut-off frequency between −20% and 50% of the original chosen frequency. This resulted in a standard deviation for the derived mobility of 7%, which is typically smaller than the standard deviation caused by the expected uncertainty of semiconductor thickness measurements [1], which is in the order of 10%. Considering the quadratic relation and using the error propagation in equation (2), the resulting standard deviation caused by thickness variations is in the order of 20% [1]. Thus, the applied correction in the frequency domain causes less deviation than to be expected from the original data set and a combined maximum deviation of 27%.

Illustrated in figure 7 is the charge carrier mobility extracted from the transient SCLC measurements of all samples with

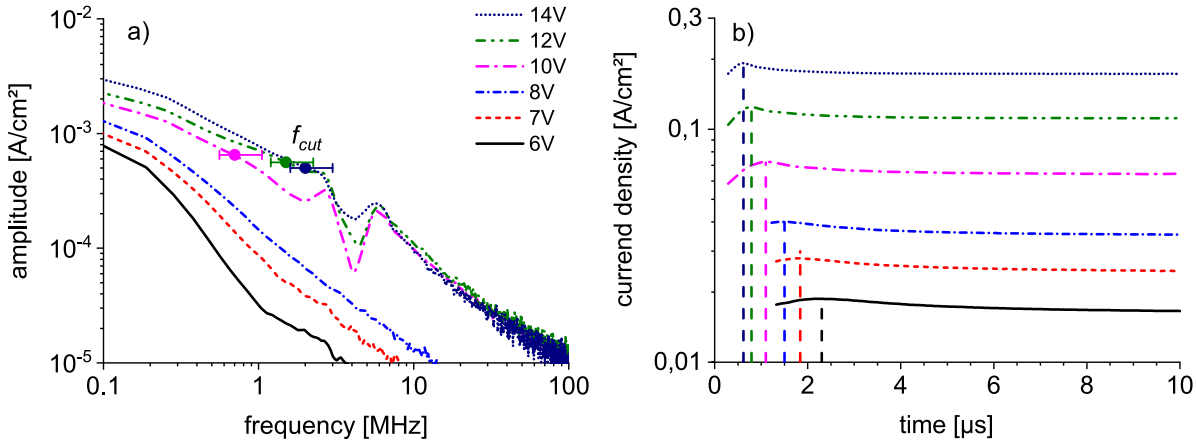

Figure 6. (a) Amplitude of the transient SCLC signals from figure 3(a) in the frequency domain, calculated by FFT. Dots mark the cut off frequency for the FFT low-pass filter used for smoothing the transient SCLC signals. For estimation of the uncertainty caused by this filtering, a range of -20% to $+50\%$ of the cut of frequency is tested and marked by horizontal bars. (b) Transient SCLC signals after smoothing.

varying thicknesses of the MTDATA layer, in correlation with the average electrical field strength. For comparison, the estimated mobility from the steady state SCLC is marked by the empty symbols on the right side of the diagram. For this estimate, equation (1) is used even for JV curves with a high gradient in the double logarithmic plot. The measured current density is considered to be reduced by the influence of the contact resistance, resulting in a lower current when compared to the ideal SCLC theory. Thus, this approach can be used as a first order estimate of the minimum mobility in the voltage range used for the fit. For a gradient larger then 3 (devices with 76 nm and 123 nm), the fit is done for the range from 1 V below the maximum voltage of the JV characteristic up to this maximum voltage. The fit has a maximum deviation by a factor of 2 when compared to the measured current density, which defines the maximum deviation of the minimum mobility. The difference between this minimum mobility and the actual mobility of the material was analyzed by Röhr *et al* [35]. For a 100 nm thin device with a 0.1 eV injection barrier, they showed that the actual mobility is five times higher then the mobility determined by equation (1). This correlates with the shown mobility differences in dependents of the semiconductor thickness in figure 7, if the injection barrier influence is neglectable for the thick layers of 642 nm and 904 nm.

Half-full symbols in figure 7 mark the mobility determined from transient SCLC without FFT correction and full symbols mark the data with FFT correction. The error bars do include the uncertainties of the applied voltage, the layer thickness of MTDATA, the manually determined t_{trans} from measured curves and the deviation caused by the FFT analysis. The deviation of the thickness measurement has the highest influence on the error bars [1], especially for thin layers, as the surface roughness is larger relative to the thickness.

Apart from these uncertainties, the errors caused by idealization of the theory, e.g. by neglecting the contact resistance or trap states are not considered, as these are not caused by the measurement circuit. However, the possible influence of non ideal devices is discussed in the following. Generally, as expected, but not accounted for in the ideal theory, the mobility

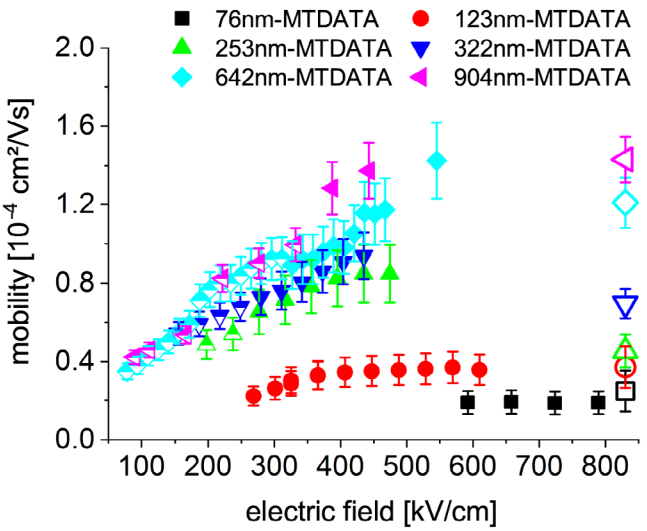

Figure 7. From TSCLC measurements calculated mobility values for different film thicknesses of MTDATA: the error bars result from deviation of the FFT filtering, reading error of the current maximum, pulse voltage and thickness uncertainty. Empty symbols mark the mobility determined by steady state SCLC, half-full symbols are measurements without FFT correction and full symbols with FFT correction.

increases with the electric field strength. Furthermore, the mobilities determined for thin layers of 76 nm and 123 nm, are much smaller than for the thicker layers. This confirms the charge injection problem already discussed for the steady state measurement. For the thicker MTDATA layers of more than 253 nm, the mobilities obtained for the different layer thicknesses are very similar to each other and in good agreement with values from the literature [10]. This proofs the accurate working principle of our circuit. The measured thin layers are in the range, where the theory has to be revised because of contact influences.

Nonetheless, the circuit provide the possibility to measure thin layers. Additionally, the high variations in sample resistances (figure 3) prove the significant flexibility of the circuit in terms of measurable currents and applicable voltages. As the

current may change strongly with the mobility and film thickness of any semiconductor type measured in a device by the circuit, the implemented wide current (0.1 μA–0.5 A) and voltage range (3.5–50 V) is a great advantage when compared to the discussed other methods. The measurable minimum mobility strongly depends on the thickness of the semiconductor. Considering a minimum t_{trans} of 300 ns and a film thickness of 100 nm, the detectable minimum mobility is 10^{-4} cm^2 Vs^{-1} (equation (2)). For a thick film of 1 μm it is 1 cm^2 Vs^{-1}.

6. Conclusion

The determination of mobility by the transient SCLC method is challenging for thin active layers due to the influence of device charging effects falsifying the measurement. Here, we have demonstrated a fast measurement circuit with a low RC time constant, which considerably reduces the influence of charging effects. At the same time, the circuit is able to measure a wide current and voltage range. Thus, the circuit allows for high flexibility in terms of minimum film thickness, device area and detectable charge carrier mobility. Additionally, the measurements with this circuit are simpler to perform than when using other methods, such as bridge circuits. We have demonstrated the working principle of this circuit using organic hole only thin films (MTDATA) and were able to measure hole mobility values of 10^{-4} cm^2 Vs^{-1} for a layer thickness down to 76 nm. Consequently, with this improvement of transient SCLC measurements, this circuit provides an easy to use characterization method for a wide range of semiconductors.

Supplementary material

The complete circuit and the PCB layout, including all used elements, are shown in the supplementary material.

Acknowledgments

The authors would like to thank the German Research Foundation (DFG) in the framework of the project ICHTIOS (SCHM 1523/8-1; BE 5104/2-1) and the program OP.EFRE of North Rhine–Westphalia and the European Union for their financial support in the framework of the Leitmarkwettbewerb 'Neue Werkstoffe' and the project PEROBOOST (EFRE-0800120).

ORCID iDs

Karsten Rojek https://orcid.org/0000-0001-7717-9270
Roland Schmechel https://orcid.org/0000-0002-5976-4975

References

[1] Blakesley J C, Castro F A, Kylberg W, Dibb G F, Arantes C, Valaski R, Cremona M, Kim J S and Kim J-S 2014 Towards reliable charge-mobility benchmark measurements for organic semiconductors *Org. Electron.* **15** 1263–72
[2] Shirota Y and Kageyama H 2007 Charge carrier transporting molecular materials and their applications in devices *Chem. Rev.* **107** 953–1010
[3] Kokil A, Yang K and Kumar J 2012 Techniques for characterization of charge carrier mobility in organic semiconductors *J. Polym. Sci.* B **50** 1130–44
[4] Lee H K, Chan K K and So S 2012 Role of electron blocking and trapping layers in transport characterization of a photovoltaic polymer poly(3-hexylthiophene) *Org. Electron.* **13** 541–4
[5] Davids P S, Campbell I H and Smith D L 1997 Device model for single carrier organic diodes *J. Appl. Phys.* **82** 6319–25
[6] Poplavskyy D and Nelson J 2003 Nondispersive hole transport in amorphous films of methoxy-spirofluorene-arylamine organic compound *J. Appl. Phys.* **93** 341–6
[7] Campbell A J, Bradley D D C, Antoniadis H, Inbasekaran M, Wu W W and Woo E P 2000 Transient and steady-state space-charge-limited currents in polyfluorene copolymer diode structures with ohmic hole injecting contacts *Appl. Phys. Lett.* **76** 1734–6
[8] Stößel M, Staudigel J, Steuber F, Blässing J, Simmerer J and Winnacker A 2000 Space-charge-limited electron currents in 8-hydroxyquinoline aluminum *Appl. Phys. Lett.* **76** 115–7
[9] Jurić I and Tutiš E 2014 Dark injection transient spectroscopy and density of states in amorphous organics *Org. Electron.* **15** 226–239
[10] So S K, Tse S C and Tong K L 2007 Charge transport and injection to phenylamine-based hole transporters for OLEDs applications *J. Disp. Technol.* **3** 225–32
[11] Esward T, Knox S, Jones H, Brewer P, Murphy C, Wright L and Williams J 2011 A metrology perspective on the dark injection transient current method for charge mobility determination in organic semiconductors *J. Appl. Phys.* **109** 093707
[12] Chiba T, Nakayama K, Pu Y, Nishina T, Yokoyama M and Kido J 2011 Hole mobility measurement of 4,4'-bis[n-(1-naphthyl)-n-phenylamino]- biphenyl by dark injection method *Chem. Phys. Lett.* **502** 118–20
[13] Szymanski M Z, Luszczynska B, Verilhac J-M, Reiss P and Djurado D 2013 Simplified transient space-charge-limited current measurements of mobility using transimpedance amplifier *Org. Electron.* **14** 230–5
[14] Paasch G and Scheinert S 2009 Space-charge-limited currents in organics with trap distributions: analytical approximations versus numerical simulation *J. Appl. Phys.* **106** 084502
[15] Mott N F and Gurney R W 1940 *Electronic Processes in Ionic Crystals* (New York: Clarendon)
[16] Lampert M A and Mark P 1970 *Current Injection in Solids* ed H G Booker and N DeClaris (New York: Academic)
[17] Many A and Rakavy G 1962 Theory of transient space-charge-limited currents in solids in the presence of trapping *Phys. Rev.* **126** 1980–8
[18] Scher H and Montroll E W 1975 Anomalous transit-time dispersion in amorphous solids *Phys. Rev.* B **12** 2455–77
[19] Chiguvare Z and Dyakonov V 2004 Trap-limited hole mobility in semiconducting poly(3-hexylthiophene) *Phys. Rev.* B **70** 1–8
[20] Steyrleuthner R, Schubert M, Jaiser F, Blakesley J C, Chen Z, Facchetti A and Neher D 2010 Bulk electron transport and charge injection in a high mobility n-type semiconducting polymer *Adv. Mater.* **22** 2799–803
[21] Agrawal R, Kumar P, Ghosh S and Mahapatro A K 2008 Thickness dependence of space charge limited current and injection limited current in organic molecular semiconductors *Appl. Phys. Lett.* **93** 073311
[22] Paasch G and Scheinert S 2007 Space charge layers in organic field-effect transistors with Gaussian or exponential semiconductor density of states *J. Appl. Phys.* **101** 024514

[23] Zubair M, Ang Y S and Ang L K 2018 Thickness dependence of space-charge-limited current in spatially disordered organic semiconductors *IEEE Trans. Electron Devices* **65** 3421–9
[24] Goldie D M 1999 Transient space-charge-limited current pulse shapes in molecularly doped polymers *J. Phys. D: Appl. Phys.* **32** 3058–67
[25] Szymanski M Z, Kulszewicz-Bajer I, Faure-Vincent J and Djurado D 2012 Comparison of simulations to experiment for a detailed analysis of space-charge-limited transient current measurements in organic semiconductors *Phys. Rev.* B **85** 195205
[26] Staudigel J 1999 Organische Leuchtdioden auf der basis Funktioneller Moleküle: Charakterisierung und Modellierung von Mehrschichtsystemen *PhD Thesis* Rhine–Westphalia-University (FAU)
[27] Texas Instruments 2013 LM6171: High Speed Low Power Low Distortion Voltage Feedback Amplifier SNOS745C *Datasheet* (www.ti.com/lit/gpn/LM6171)
[28] Heraeus Deutschland GmbH & Co. 2016 Clevios HIL-E 100 81108992 *Datasheet* (http://www.heraeus.com/media/media/hec/documents_hec/data_sheets_hep/81108992_PD_Clevios_HIL_E_100.pdf)
[29] Adachi C, Kwong R and Forrest S R 2001 Efficient electrophosphorescence using a doped ambipolar conductive molecular organic thin film *Org. Electron.* **2** 37–43
[30] Yan X *et al* 2013 Improved photovoltaic characteristics of organic cells with heterointerface layer as a hole-extraction layer inserted between ito anode and donor layer *Org. Electron.* **14** 1805–1810
[31] Baldo M A and Forrest S R 2001 Interface-limited injection in amorphous organic semiconductors *Phys. Rev.* B **64** 085201
[32] Ishii H, Sugiyama K, Ito E and Seki K 1999 Energy level alignment and interfacial electronic structures at organic/metal and organic/organic interfaces *Adv. Mater.* **11** 605–25
[33] Silver M, Mark P, Olness D, Helfrich W and Jarnagin R C 1962 On the observation of transient space-charge-limited currents in insulators *J. Appl. Phys.* **33** 2988–91
[34] Cooley J W and Tukey J W 1965 An algorithm for the machine calculation of complex Fourier series *Math. Comput.* **19** 249–59
[35] Röhr J A, Moia D, Haque S A, Kirchartz T and Nelson J 2018 Exploring the validity and limitations of the Mott–Gurney law for charge-carrier mobility determination of semiconducting thin-films *J. Phys.: Condens. Matter* **30** 105901